World Scientific
www.worldscientific.com

Binary organic nanoparticles with enhanced reactive oxygen species generation capability for photodynamic therapy

Xiaofu Weng[*], Zhouzhou Bao[†,‡,§] and Xunbin Wei[*,¶]

*School of Biomedical Engineering
Shanghai Jiao Tong University
Shanghai 200030, P. R. China*

†*Department of Obstetrics and Gynecology
Ren Ji Hospital, School of Medicine
Shanghai Jiao Tong University
Shanghai 200127, P. R. China*

‡*Shanghai Key Laboratory of
Gynecologic Oncology
Ren Ji Hospital, School of Medicine
Shanghai Jiao Tong University
Shanghai 200127, P. R. China*
§*baozhouzhou@126.com*
¶*xwei01@sjtu.edu.cn*

Photodynamic therapy (PDT) takes advantage of photosensitizers (PSs) to generate reactive oxygen species (ROS) for cell killing when excited by light. It has been widely used in clinic for therapy of multiple cancers. Currently, all the FDA-approved PSs, including porphyrin, are all small organic molecules, suffering from aggregation-caused quenching (ACQ) issues in biological environment and lacking tumor targeting capability. Nanoparticles (NPs) with size between 20 nm and 200 nm possess tumor targeting capability due to the enhanced permeability and retention (EPR) effect. It is urgent to develop a new strategy to form clinical-approved-PSs-based NPs with improved ROS generation capability. In this study, we report a strategy to overwhelm the ACQ of porphyrin by doping it with a type of aggregation-induced emission (AIE) luminogen to produce a binary NPs with high biocompatibility, and enhanced fluorescence and ROS generation capability. Such NPs can be readily synthesized by mixing a porphyrin derivative, Ce6 with a typical AIE luminogen, TPE-Br. Here, our experimental results have demonstrated the feasibility and effectiveness of this strategy, endowing it a great potential in clinical applications.

Keywords: Aggregation-induced emission; photodynamic therapy; organic nanoparticles.

§,¶Corresponding authors.

1. Introduction

Cancer is the second leading cause of mortality globally. In addition to radiotherapy, chemotherapy, and surgery, various emerging treatment strategies have been proposed.[1–6] Photodynamic therapy (PDT) has attracted much attention in recent years, due to its high spatiotemporal precision, low side-effect, noninvasive properties, etc.[7,8] It relies on photosensitizers (PSs) and light to generate reactive oxygen species (ROS) to destroy the target cells or tissue. In recent years, various PSs have been designed and synthesized for cancer therapy.[9,10] Porphyrin and its derivatives are still the most widely used PSs.[11–13] However, these PSs normally possess hydrophobic and planar π-conjugated structures and consequently suffer from aggregation-caused quenching (ACQ) issue in aqueous media.[14] According to the Jablonski diagram, after the PS molecule absorbs the excitation light, there are generally three energy dissipation pathways: the excited singlet state to fluorescence emission pathway, intersystem crossing (ISC) to a triplet excited state for PDT, and thermal deactivation pathway via nonradiative decay.[15] As the three dissipation pathways of absorbed excitation energy are always competing, the optimized efficacy of the required phototheranostic function can be realized by suppression of the other pathways. Due to the hydrophobic and rigid planar structures, most PSs can easily aggregate in aqueous media and result in the excited state energy dissipation in nonradiative decay pathway and consequently reduced PDT efficiency.[16] Thus, it is thought that PDT has not reached its full potential. It is essential to develop high performance PSs for efficient PDT.

Nanoparticles (NPs) with unique properties that only exhibit at nanoscales have been developed very fast and widely used in biomedical researches and applications.[17,18] The chemical and physical characters of nanoscale materials are significantly different from those of macroscales materials, therefore providing novel and powerful functions.[19] Specifically, the surface of NPs can be coated with biocompatible molecules to combine with target cells or tissue and tune the solubility.[20,21] In this way, the NPs are capable of being modified with multiple predesigned functions.[22,23] The high surface-to-volume ratio further brings large contact area, high-efficiency molecular reactions, and thus promising potential in biomedical applications.[24,25]

Plenty of different types of NPs have been developed for tumor diagnostics and therapy.[26–28] The microvascular epithelial cells in most normal tissue contact tightly with each other with little interspace. Molecules and lipid granules can hardly pass through the vessel walls. In contrast, the blood vessels in the tumor are usually lacking in integrity. Molecules and other nanoscale materials can directly diffuse out from the blood and stay in the tumor tissue, so-called the enhanced permeability and retention (EPR) effect.[29,30] Similarly, the NPs injected into blood vessels, ranging from 20 nm to 200 nm, can also be enriched in tumors by such EPR effect. In this regard, the NPs at the scale of 10 nm are naturally targeted to tumor tissue, which can further be combined with other technologies for targeted photothermal therapy (PTT), PDT, and immune therapy of cancer.[31–33]

However, due to the inherent ACQ issue, low concentration of porphyrin and its derivatives are integrated with drug carriers, including mesoporous silica, two-dimensional nanomaterials, etc., to relieve ACQ and realize tumor targeting. However, the biosafety of inorganic nanomaterials is still concerned.[34] Thus, it is of great importance to develop a new strategy to form clinically-approved-PSs-based NPs with improved ROS generation capability and tumor-targeting capability.

PSchlorin e6 (Ce6), an FDA-approved second-generation PS, which can effectively generate singlet oxygen ($^1O_2$) under light irradiation, is extensively used in PDT.[35] Despite these upsides, Ce6 has shortcomings including poor water solubility and being easy to aggregate, which largely compromise its therapeutic efficacy. Strategies of combination with nanomaterials for improving the dispersion of Ce6, like encapsulating Ce6 with metal organic framework, carrying Ce6 with two-dimensional carrier, loading Ce6 by supramolecular hydrogels, and anchoring with gold nanostructures for PDT, have been reported.[36] While these methods achieved effective anticancer performance, these nanoagents still suffered from tedious preparation process, poor degradation, and potential toxicity.

The recently discovered aggregation-induced emission (AIE) fluorogenic (AIEgens) molecules, which are observed in molecules with rotating units such as phenyl rings, have non-coplanar benzene rings with steric hindrance, making them promising blockers for overcoming ACQ. AIEgens have also been designed to serve as phototherapy reagents by

facilitating the ISC process.[37] By incorporating electron donors and acceptors into π-conjugated systems to optimize the ISC process, the ROS quantum yield of AIEgens could reach 0.89. In addition, AIEgens are used as core component for enhancing fluorescence quantum yield for promising cellular and vascular imaging.[25] The clinical application barrier is the biosafety of AIEgens, which is under investigations. Currently, there are no reports on using AIEgens as building blocks to simultaneously enhance ROS generation capacity and fluorescence quantum yield.

In this study, binary organic NPs (BONPs) composed of two components (TPE-Br and Ce6) are synthesized for efficient PDT. The two components are encapsulation with amphiphilic 1,2-distearoyl-sn-glycero-3-phosphoethanolamine-N-amino (polyethylene glycol)-2000 (DSPE-mPEG) to obtain NPs with excellent dispersion. By increasing the molar ratio of TPE-Br/Ce6, the ROS generation capacity and fluorescence quantum yield of Ce6 are improved. The enhancement of ROS generation yield ensures efficient PDT in Hela cells. Without changing the molecular structures, there are no required tedious synthesis and postprocessing. This strategy of obtaining BONPs has provided a simple method for elevating the performance of therapeutic agents.

2. Methods and Results

2.1. *The synthesis and characterization of Ce6+TPE-Br@DSPE-mPEG NPs*

In this study, to design a biocompatible tumor-targeting PDT PS, the porphyrin derivative, Ce6, needs to be coated with DSPE-mPEG to produce NPs with EPR effect. To decrease ACQ of Ce6 and enhance the ROS generation, the AIEgen, TPE-Br is doped inside to prevent the π-π stack of molecules while its fluorescence spectrum is far from that of Ce6. In this regard, three types of NPs were designed and synthesized (all coated with DSPE-mPEG) as follows: (1) Ce6 NPs (solely Ce6); (2) BONPs with both Ce6 and TPE-Br (doping ratio of Ce6: TPE-Br ∼ 1:12); and (3) BONPs (Ce6: TPE-Br ∼ 1:24). The Ce6 concentration in all those three NPs was consistently 2 μM. Generally, the synthesis of those NPs followed the protocol. DSPE-mPEG was added directly into the mixture of 200 μL Ce6

(200 μM) and 0, 200, or 400 μL TPE-Br (2400 μM), and then tetrahydrofuran (THF) solution to 2 mL. The mixture was then injected into 20 mL ultrapure water, shaken by ultrasonic wave for 2 min, and stirred for evaporation of THF. The NPs could be harvested after overnight stewing. The protocol was briefly introduced in Fig. 1(a). The NP size was measured by dynamic light scattering (DLS) method (Fig. 1(b)). The diameter of Ce6 NPs and BONPs were 36 nm and 43 nm, respectively. The obtained size guaranteed the *in vivo* tumor targeting via EPR effect.

The planar π-conjugated PS molecules are always resulting in quenched fluorescence in the aggregation state due to the hydrophobic and rigid planar structures. In order to alleviate the ACQ effect of NPs composed of organic PSs, AIEgens of TPE-Br was selected to co-dope with PSs to form the binary NPs. The non-coplanar structure of AIEgens were expected to separate the PSs in the NPs, efficiently lowering the ACQ effect. Thus, the organic PSs and AIEgens were carefully selected in consideration of the spectral characteristics. Ce6 and TPE-Br were chosen because there was no significant spectral overlap between the emission of TPE-Br and absorption of Ce6. The measured spectra of Ce6 and TPE-Br NPs were shown in Fig. 1(c). It should be noted that the excitation peak of Ce6 and TPE-Br was 405 nm and 320 nm respectively, which could guarantee the excitation of Ce6 but prevent TPE-Br from being excited when exciting those NPs at 400–700 nm. The original fluorescence peak of Ce6 NPs was at around 460 nm. The peak moved to 680 nm in the presence of TPE-Br. If the TPE-Br concentration was increased during the synthesis of BONPs, fluorescence emission at 680 nm was significantly enhanced (Fig. 1(d)).

To measure the ROS generation of those NPs, ROS indicator of 9,10-anthracenediyl-bis (methylene) dimalonic acid (ABDA, final concentration: 50 μM) was added into the NP solutions. The absorption spectra of the mixture of TPE-Br@DSPE-mPEG (48 μM) and ABDA under the irradiation by white light (400–700 nm at 100 mW/cm^2) were measured as shown in Fig. 2(a). The absorption peak located at 400 nm almost kept constant, eliminating any interference from TPE-Br. While for the pure Ce6 NPs as shown in Fig. 2(b), the absorption peak located at 400 nm decreased slightly since ACQ issue remarkably decreased the
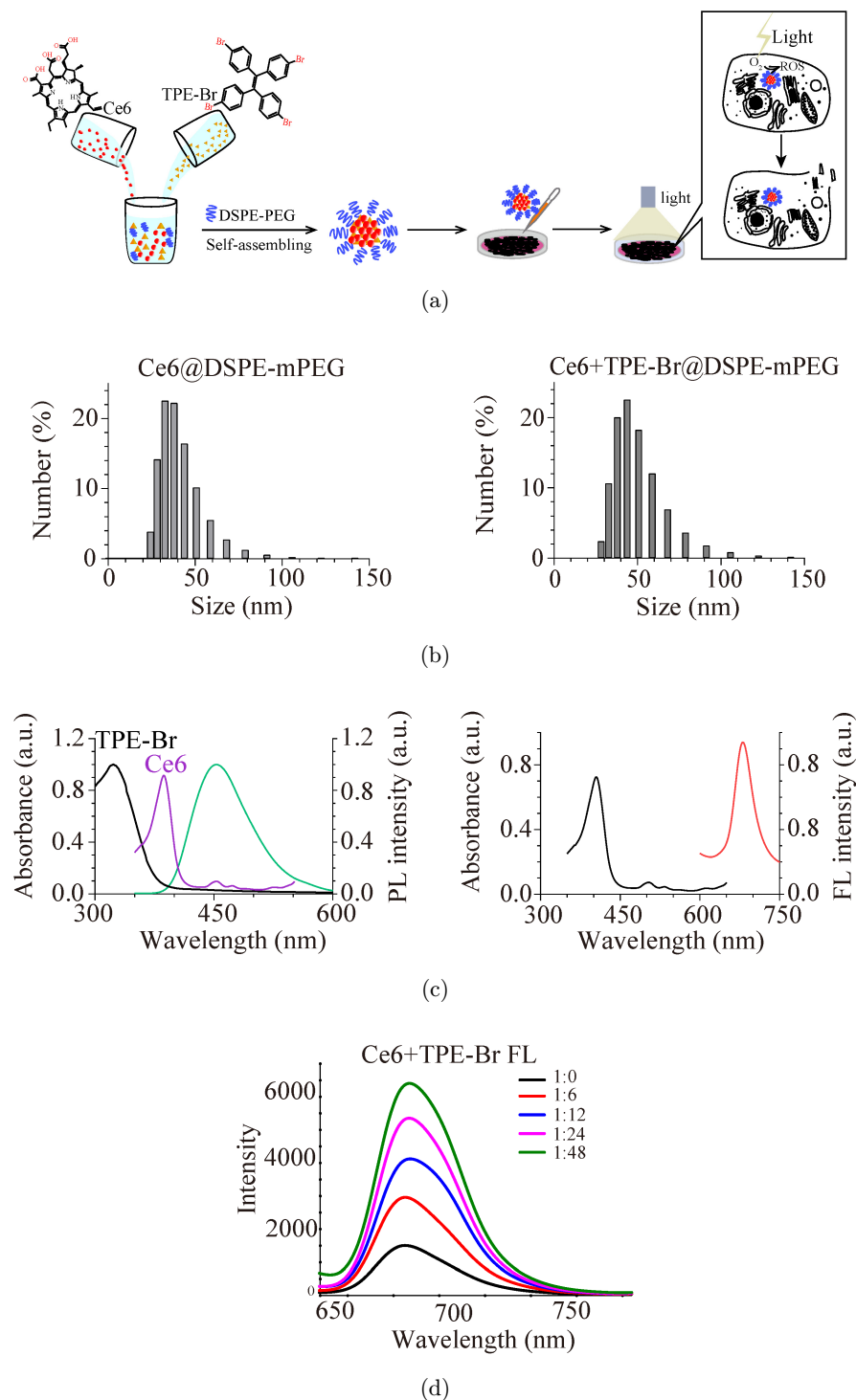
Fig. 1. The size and fluorescence spectrum of BONPs. (a) The brief protocol to synthesis the BONPs for PDT. (b) The size distribution of Ce6 NPs (left) and BONPs (right) NPs. (c) The optical spectral characteristics of TPE-Br NPs (left) and BONPs (right). (d) The fluorescence spectrum of BONPs NPs with different doping ratio of TPE-Br.

ROS generation capability. Once the Ce6 molecule was separated by doped TPE-Br, the ACQ was efficiently alleviated. As shown in Figs. 2(c) and 2(d), the absorption peak located at 400 nm were apparently lowered with the 1:12 and 1:24 doping ratio of TPE-Br. The quantum yield of Ce6 +TPE-Br NPs at 1:24 doping ratio was measured as in Fig. 2(e), which remained stable in 24 h.
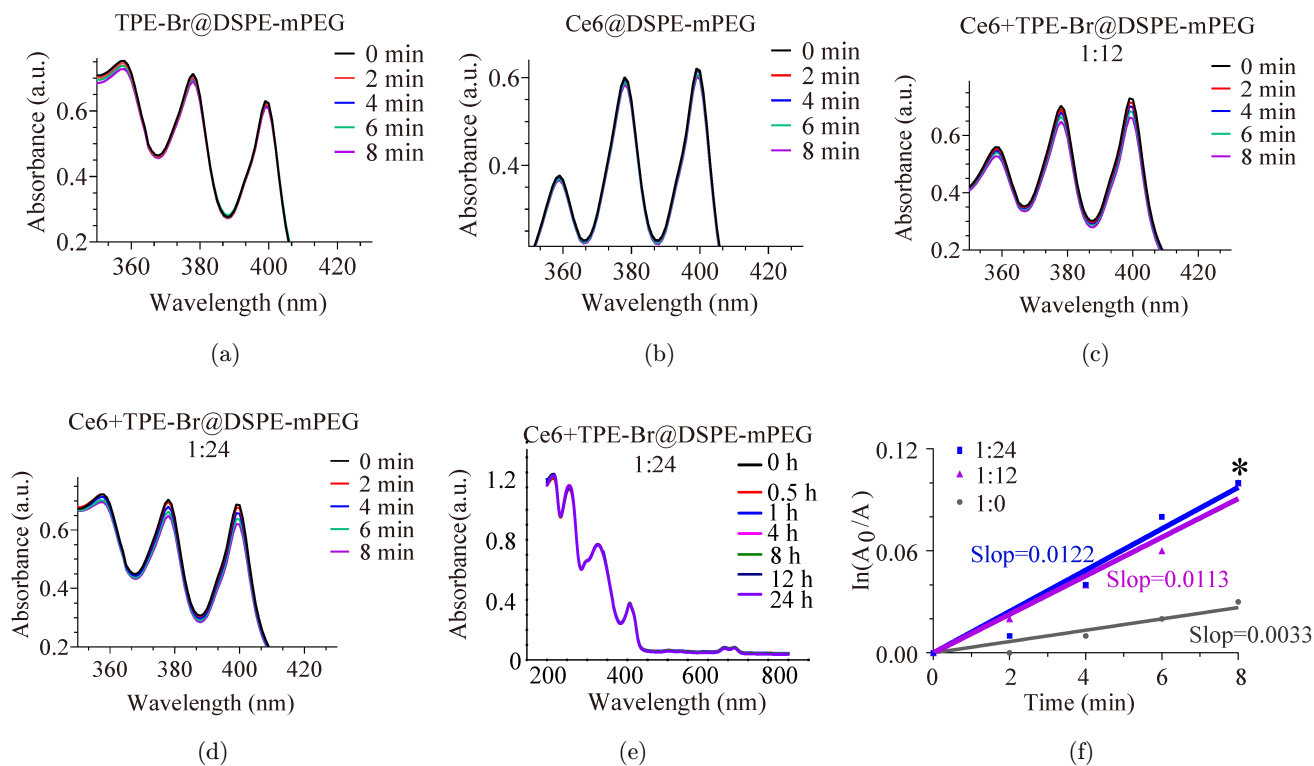
Fig. 2. The fluorescence enhancement and ROS production by BONPs. The fluorescence spectrum of TPE-Br NPs (a), Ce6 NPs (b), Ce6+TPE-Br (1:12) NPs (c), and Ce6+TPE-Br (1:24) NPs (d) indicate the enhancement of fluorescence emission. (e) The quantum yield of Ce6+TPE-Br at 1:24 in 24 h. (f) The ABDA degradation by Ce6 NPs, Ce6+TPE-Br (1:12) NPs, and Ce6+TPE-Br (1:24) NPs under white light excitation. The slopes of time-lapse degradation of those NPs were acquired by linear fitting. *$p < 0.05$ by students' t-test.

The ROS generation capability of this binary NPs was enhanced 3-fold as compared with the pure Ce6 NPs, and could be further improved by increasing the doping ratio (Fig. 2(f)). Thus the formed binary NPs have improved ROS generation and tumor-targeting capability, making binary NPs promising for clinical applications.

2.2. *PDT effect by BONPs*

HeLa cells are cervical cancer cell lines, while cervical cancer is one of the major diseases threatening human health worldwide. Thus, this work chooses HeLa cells for evaluating the biocompatibility and PDT efficacy of BONPs. Before performing the *in vitro* cancer cell study, the biocompatibility of binary NPs was investigated. HeLa cells were incubated with NPs of different concentrations for 48 h when viability test was performed. The cells were seeded into 96-well plates, around 5000 cells in each well. After cells were adhered on the bottom, the cell buffer was replaced with culture medium with different concentrations of BONPs (0.5, 1.0, 1.5,

2.0, 2.5, and 3.0 μM). The cells were then cultured for 24 h and 48 h, and washed by PBS before incubation with 100 μL CCK-8 at 37°C for 2 h. The absorption of the cell solutions at 450 nm was finally measured by a Microplate Reader (Bio-Tek Synergy HT). As shown in Fig. 3(a), the cell viability incubated with each concentration of BONPs was not totally influenced in 48 h, implying an excellent biocompatibility.

Next, HeLa cells incubated with BONPs for 12 h were irradiated by white light (400–700 nm, 100 mW/cm^2) for 15 min. After the treatment, cells were incubated with fresh medium for another 5 h and stained with Calcein-AM and PI for live/dead cell staining. As shown in Fig. 3(b), cells treated with only white light irradiation or only NPs showed green fluorescence of Calcein-AM, eliminating the light irradiation interference and demonstrating the excellent biocompatibility of NPs. Meanwhile, in the PDT group, not any PI signal was observed in the cells treated with 2.0 μM Ce6 NPs under white light irradiation, indicating not any cellular phototoxicity. It meant that the Ce6
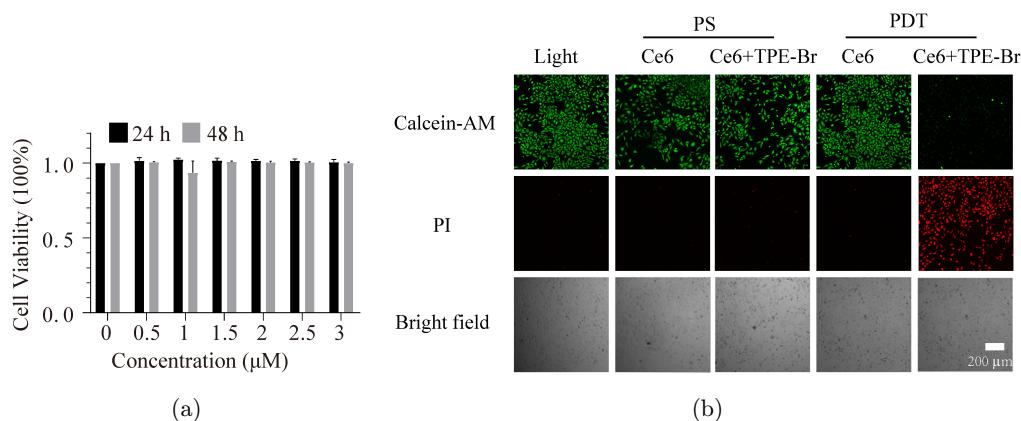
Fig. 3. The PDT test of BONPs. (a) Cell viability tested by CCK8 after incubation with different concentrations of BONPs for 24 h or 48 h. (b) PDT test of HeLa cells incubated with BONPs. Light: HeLa cells solely suffered irradiation of white light without any NPs. PS: cells incubated with only Ce6 or BONPs without any light irradiation. PDT: Cells incubated with Ce6 and BONPs and treated with light irradiation. Calcein-AM (Ex: 488 nm; Em: 505–525 nm) and propidium iodide (PI) (Ex: 552 nm; Em: 605–625 nm).

Table 1. The general potential in clinical PDT of BONPs.

PDT drug	Anti-ACQ	ROS enhancement	Tumor target	Clinic potential	Synthesis
Porphyrin	No	No	Moderate	Clinic	Easy
ALA	No	No	Moderate	Clinic	Easy
BONPs	Yes	Yes	EPR	Good	Easy

NPs non-doped with TPE-Br could not generate ROS due to the ACQ issue, while strong PI signal was observed in the cells treated with both binary NPs and light irradiation. The superior cancer cell ablation capability of binary NPs makes it a great promising candidate for clinical cancer treatment.

3. Conclusion

In this study, we proposed a general strategy to alleviate the ACQ of organic PS formed NPs by inducing AIEgen to separate PS molecular. As compared with pure Ce6 NPs, the ROS generation capability of formed binary NPs was remarkably increased, while the excellent cancer cell ablation by PDT using binary NPs was achieved. Furthermore, developed binary NPs possessed unique advantages including high ROS generation efficiency, excellent biocompatibility, making binary NPs promising in practical PDT applications, as generalized in Table 1. This study highlights the general strategy to achieve organic PSs NPs with improved ROS generation capability for future translational research.

Conflict of Interest

The authors declare no competing financial interests.

Acknowledgments

References

1. Y. Sun, F. Ding, Z. Chen, R. Zhang, C. Li, Y. Xu, Y. Zhang, R. Ni, X. Li, G. Yang, Y. Sun, P. J. Stang, "Melanin-dot-mediated delivery of metallacycle for NIR-II/photoacoustic dual-modal imaging-guided chemo-photothermal synergistic therapy," *Proc. Natl. Acad. Sci. USA* **116**, 16729–16735 (2019).

2. Y. Xu, Y. Zhang, J. Li, J. An, C. Li, S. Bai, A. Sharma, G. Deng, J. S. Kim, Y. Sun, "NIR-II emissive multifunctional AIEgen with single laser-activated synergistic photodynamic/photothermal therapy of cancers and pathogens," *Biomaterials* **259**, 120315 (2020).

3. J. Li, Y. Liu, Y. Xu, L. Li, Y. Sun, W. Huang, "Recent advances in the development of NIR-II organic emitters for biomedicine," *Coord. Chem. Rev.* **415**, 213318 (2020).

4. L. Tu, Y. Xu, Q. Ouyang, X. Li, Y. Sun, "Recent advances on small-molecule fluorophores with emission beyond 1000 nm for better molecular imaging *in vivo*," *Chin. Chem. Lett.* **30**, 1731–1737 (2019).

5. A. Abdurashitov, V. Tuchin and O. Semyachkina-Glushkovskaya, "Photodynamic therapy of brain tumors and novel optical coherence tomography strategies for *in vivo* monitoring of cerebral fluid dynamics," *J. Innov. Opt. Health Sci.* **13**, 2030004 (2020).

6. S. Huang, C. I. Fong, M. Xu, B.-N. Han, Z. Yuan, Q. Zhao, "Nano-loaded natural killer cells as carriers of indocyanine green for synergetic cancer immunotherapy and phototherapy," *J. Innov. Opt. Health Sci.* **12**, 1941002 (2019).

7. D. W. Felsher, "Photodynamic therapy for cancer," *Nat. Rev. Cancer* **3**, 375–80 (2003).

8. Z. Huang, H. P. Xu, A. D. Meyers, A. I. Musani, L. W. Wang, R. Tagg, A. B. Barqawi, Y. K. Chen, "Photodynamic therapy for treatment of solid tumors — Potential and technical challenges," *Technol. Cancer Res. Treat.* **7**, 309–320 (2008).

9. M. H. Lan, S. J. Zhao, W. M. Liu, C. S. Lee, W. J. Zhang, P. F. Wang, "Photosensitizers for photodynamic therapy," *Adv. Healthc. Mater.* **8**, 1900132 (2019).

10. D. Chen, M. Song, J. Huang, N. Chen, J. Xue and M. Huang, "Photocyanine: A novel and effective phthalocyanine-based photosensitizer for cancer treatment," *J. Innov. Opt. Health Sci.* **13**, 2030009 (2020).

11. J. Li, W. Sun, Z. Yang, G. Gao, H.-H. Ran, K.-F. Xu, Q.-Y. Duan, X. Liu, F.-G. Wu, "Rational design of self-assembled cationic porphyrin-based nanoparticles for efficient photodynamic inactivation of bacteria," *ACS Appl. Mater. Interfaces* **12**, 54378–54386 (2020).

12. A. Sulek, B. Pucelik, M. Kobielusz, A. Barzowska, J. M. Dabrowski, "Photodynamic inactivation of bacteria with porphyrin derivatives: Effect of charge, lipophilicity, ROS generation, and cellular uptake on their biological activity *in vitro*," *Int. J. Mol. Sci.* **21**, 8716 (2020).

13. J. Tian, B. X. Huang, M. H. Nawaz, W. A. Zhang, "Recent advances of multi-dimensional porphyrin-based functional materials in photodynamic therapy," *Coord. Chem. Rev.* **420**, 213410 (2020).

14. G. X. Feng, B. Liu, "Aggregation-induced emission (AIE) dots: Emerging theranostic nanolights," *Acc. Chem. Res.* **51**, 1404–1414 (2018).

15. H. Qian, M. E. Cousins, E. H. Horak, A. Wakefield, M. D. Liptak, I. Aprahamian, "Suppression of Kasha's rule as a mechanism for fluorescent molecular rotors and aggregation-induced emission," *Nat. Chem.* **9**, 83–87 (2017).

16. Y. Hong, J. W. Lam, B. Z. Tang, "Aggregation-induced emission," *Chem. Soc. Rev.* **40**, 5361–5388 (2011).

17. W. Fan, B. Yung, P. Huang, X. Chen, "Nanotechnology for multimodal synergistic cancer therapy," *Chem. Rev.* **117**, 13566–13638 (2017).

18. B. R. He, B. Situ, Z. J. Zhao, L. Zheng, "Promising applications of AIEgens in animal models," *Small Methods* **4**, 1900583 (2020).

19. X. H. Gao, Y. Y. Cui, R. M. Levenson, L. W. K. Chung, S. M. Nie, "*In vivo* cancer targeting and imaging with semiconductor quantum dots," *Nat. Biotechnol.* **22**, 969–976 (2004).

20. O. Bolton, K. Lee, H. J. Kim, K. Y. Lin, J. Kim, "Activating efficient phosphorescence from purely organic materials by crystal design," *Nat. Chem.* **3**, 205–210 (2011).

21. R. Bakalova, Z. Zhelev, I. Aoki, H. Ohba, Y. Imai, I. Kanno, "Silica-shelled single quantum dot micelles as imaging probes with dual or multimodality," *Anal. Chem.* **78**, 5925–5932 (2006).

22. X. W. Hua, Y. W. Bao, F. G. Wu, "Fluorescent carbon quantum dots with intrinsic nucleolus-targeting capability for nucleolus imaging and enhanced cytosolic and nuclear drug delivery," *ACS Appl. Mater. Interfaces* **10**, 10664–10677 (2018).

23. N. Panwar, A. M. Soehartono, K. K. Chan, S. W. Zeng, G. X. Xu, J. L. Qu, P. Coquet, K. T. Yong and X. Y. Chen, "Nanocarbons for biology and medicine: Sensing, imaging, and drug delivery," *Chem. Rev.* **119**, 9559–9656 (2019).

24. S. Kato, T. Matsumoto, T. Ishi, T. Thiemann, M. Shigeiwa, H. Gorohmaru, S. Maeda, Y. Yamashita, S. Mataka, "Strongly red-fluorescent novel donor-pi-bridge-acceptor-pi-bridge-donor (D-pi-A-pi-D) type 2,1,3-benzothiadiazoles with enhanced two-photon absorption cross-sections," *Chem. Commun.* **2004**, 2342–2343 (2004).

25. M. Liu, B. Gu, W. Wu, Y. Duan, H. Liu, X. Deng, M. Fan, X. Wang, X. Wei, K.-T. Yong, K. Wang, G. Xu, B. Liu, "Binary organic nanoparticles

with bright aggregation-induced emission for three-photon brain vascular imaging," *Chem. Mater.* **32**, 6437–6443 (2020).

26. J. C. Ge, Q. Y. Jia, W. M. Liu, M. H. Lan, B. J. Zhou, L. Guo, H. Y. Zhou, H. Y. Zhang, Y. Wang, Y. Gu, X. M. Meng, P. F. Wang, "Carbon dots with intrinsic theranostic properties for bioimaging, red-light-triggered photodynamic/photothermal simultaneous therapy *in vitro* and *in vivo*," *Adv. Healthc. Mater.* **5**, 665–675 (2016).

27. W. Pang, P. Jiang, S. Ding, Z. Bao, N. Wang, H. Wang, J. Qu, D. Wang, B. Gu, X. Wei, "Nucleolus-targeted photodynamic anticancer therapy using renal-clearable carbon dots," *Adv. Healthc. Mater.* **9**, e2000607 (2020).

28. S. S. Lucky, K. C. Soo, Y. Zhang, "Nanoparticles in photodynamic therapy," *Chem. Rev.* **115**, 1990–2042 (2015).

29. Y. Zhu, W. J. Tong, C. Y. Gao, H. Mohwald, "Fabrication of bovine serum albumin microcapsules by desolvation and destroyable cross-linking," *J. Mater. Chem.* **18**, 1153–1158 (2008).

30. W. Qin, D. Ding, J. Z. Liu, W. Z. Yuan, Y. Hu, B. Liu, B. Z. Tang, "Biocompatible nanoparticles with aggregation-induced emission characteristics as far-red/near-infrared fluorescent bioprobes for *in vitro* and *in vivo* imaging applications," *Adv. Funct. Mater.* **22**, 771–779 (2012).

31. Y. Jiang, J. Li, Z. Zeng, C. Xie, Y. Lyu, K. Pu, "Organic photodynamic nanoinhibitor for synergistic cancer therapy," *Angew. Chem. Int. Ed. Engl.* **58**, 8161–8165 (2019).

32. B. J. Zhou, Y. Z. Li, G. L. Niu, M. H. Lan, Q. Y. Jia, Q. L. Liang, "Near-infrared organic dye-based nanoagent for the photothermal therapy of cancer," *ACS Appl. Mater. Interfaces* **8**, 29899–29905 (2016).

33. J. M. Liang, R. X. Li, Y. W. He, C. L. Ling, Q. Wang, Y. Z. Huang, J. Qin, W. G. Lu, J. X. Wang, "A novel tumor-targeting treatment strategy uses energy restriction via co-delivery of albendazole and nanosilver," *Nano Res.* **11**, 4507–4523 (2018).

34. F. Yin, B. Gu, Y. Lin, N. Panwar, S. C. Tjin, J. Qu, S. P. Lau, K.-T. Yong, "Functionalized 2D nano-materials for gene delivery applications," *Coord. Chem. Rev.* **347**, 77–97 (2017).

35. M. G. Adimoolam, A. Vijayalakshmi, M. R. Nalam, M. V. Sunkara, "Chlorin e6 loaded lactoferrin nanoparticles for enhanced photodynamic therapy," *J. Mater. Chem. B* **5**, 9189–9196 (2017).

36. Y. Xu, R. He, D. Lin, M. Ji, J. Chen, "Laser beam controlled drug release from Ce6–gold nanorod composites in living cells: A FLIM study," *Nanoscale* **7**, 2433–2441 (2015).

37. S. Xu, Y. Yuan, X. Cai, C.-J. Zhang, F. Hu, J. Liang, G. Zhang, D. Zhang, B. Liu, "Tuning the singlet-triplet energy gap: A unique approach to efficient photosensitizers with aggregation-induced emission (AIE) characteristics," *Chem. Sci.* **6**, 5824–5830 (2015).